Experimental and theoretical study of line mixing in methane spectra. I. The N2-broadened v3 band at room temperature

D. Pieroni, Nguyen-Van-Thanh, C. Brodbeck, C. Claveau, A. Valentin et al.

Additional information on J. Chem. Phys.
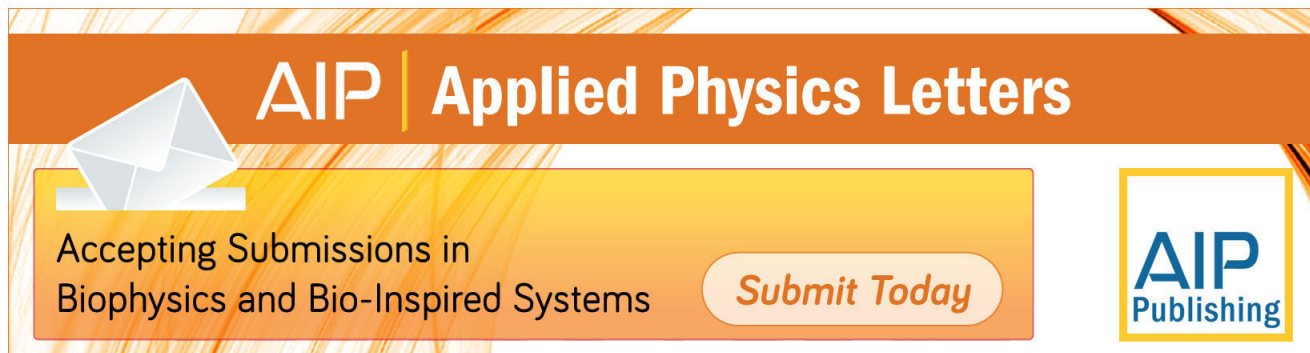
Experimental and theoretical study of line mixing in methane spectra. I. The N$_2$-broadened ν_3 band at room temperature

D. Pieroni, Nguyen-Van-Thanh, and C. Brodbeck
Laboratoire de Physique Moléculaire et Applications, UPR 136 du CNRS, Université Paris Sud, 91405 Orsay Cedex, France

C. Claveau and A. Valentin
Laboratoire de Physique Moléculaire et Applications, UPR 136 du CNRS, Université P. et M. Curie, 4 Place Jussieu, 75252 Paris Cedex 05, France

J. M. Hartmann[a)]
Laboratoire de Physique Moléculaire et Applications, UPR 136 du CNRS, Université Paris Sud, 91405 Orsay Cedex, France

T. Gabard and J.-P. Champion
Laboratoire de Physique de l'Université de Bourgogne, Unité associée au CNRS, 9 Avenue Alain Savary, B. P. 400, 21011, Dijon Cedex, France

D. Bermejo and J.-L. Domenech
Instituto de Estructura de la Materia, Consejo Superior de Investigaciones Científicas, Serrano 123, 28006 Madrid, Spain

Line-mixing effects have been studied in the ν_3 band of CH$_4$ perturbed by N$_2$ at room temperature. New measurements have been made and a model is proposed which is not, for the first time, strictly empirical. Three different experimental set ups have been used in order to measure absorption in the 2800–3200 cm^{-1} spectral region for total pressures in the 0.25–2 and 25–80 atm ranges. Analysis of the spectra demonstrates the significant influence of line mixing on the shape of the Q branch and of the P and R manifolds. A model is proposed which is based on state-to-state collisional transfer rates calculated from the intermolecular potential surface with a semiclassical approach. The line-coupling relaxation matrix is constructed from these data and two additional parameters which are fitted on measured absorption. Comparisons between measurements and spectra computed accounting for and neglecting line mixing are made. They prove the quality of the approach which satisfactory accounts for the effects of pressure and of rotational quantum numbers on the spectral shape under conditions where modifications introduced by line mixing are important. For high rotational quantum number lines, the main features induced by collisions are predicted but some discrepancies remain; the latter may be due to improper line-coupling elements but there is strong evidence that the use of inaccurate line broadening parameters also contributes to errors in calculated spectra. © *1999 American Institute of Physics.* [S0021-9606(99)00116-6]

I. INTRODUCTION

Methane is present in our atmosphere and in those of planets such as Jupiter. Knowledge of the associated amounts (mixing ratios) is required for the understanding of processes such as ozone depletion, global warming, or the formation of giant planets. The vertical distributions of CH$_4$ (or integrated total column amounts) are generally determined by using remote sensing infrared experiments (e.g., Refs. 1–3). The quality of the retrieved quantities relies on the precision of the forward modeling of the magnitude and shape of the absorption. For these reasons, the last years have been the witnesses of an increasing number of experimental and theoretical studies on the spectroscopic parameters of methane (see Ref. 4, and references therein). Much attention has been given to the line positions and intensities as well as

to the collisional parameters of isolated lines (pressure-broadening and -shifting coefficients). On the other hand, only few results are available concerning the effects of line mixing on the spectral shape, although the total pressure in the troposphere and lower stratosphere is sufficiently high to make the usual addition of Voigt (Lorentz) shapes inadequate.

To our knowledge, the first work evidencing line-mixing effects in CH$_4$ is a Raman study of the $2\nu_2$ Q branch.[5] In the infrared region, Pine reported a study[6] of the Q branch of the ν_3 band of CH$_4$ where he remarked that the addition of individual (Voigt and Rautian) line contributions failed in fitting the absorption above a few tenths of a bar. This problem was attributed to line mixing without further analysis. Latter on, multispectrum fits of high resolution Fourier transform spectra in the ν_3 region[7] were improved by introducing line mixing using the first order approach of Rosenkranz;[8] line-broadening and line-shifting coefficients were obtained with

---
[a)]Author to whom correspondence should be addressed. Tel: 33169157514; Fax: 33169157530; electronic mail: jean-michel.hartmann@lpma.u-psud.fr

TABLE I. Groups and laboratory instruments involved in the measurements.

Group→location	G_1 LPMA-Orsay	G_2 LPMA-Paris	G_3 IEM-Madrid
Instrument	FT (Bruker IFS66V)	FT (homemade)	TDFS
Used resolution	0.12 cm^{-1}	≈0.01 cm^{-1}	≈10^{-4} cm^{-1}
Pathlength (cm)	4.78–215	407–2007	64.5
$P(CH_4)$ range (mb)	0.03–13	0.04–8	0.1–36
$P(N_2)$ (atm)	25,50,80	0.5,1.0	0.25,0.5,1.,2.
Regions	P,Q,R for $J \leqslant 18$	P,Q,R for $J \leqslant 15$	R for $J=8,10,12,14,16$

increased precision but no quantitative information was published on line coupling. The first study providing data in order to account for line mixing is given in Ref. 9. In this work, N_2 and Ar broadened spectra of the ν_3 P- and R-branch manifolds for $J \leqslant 10$ were recorded at pressures below the atmosphere. They were fitted using the Rosenkranz perturbation treatment and neglecting[10] coupling between transitions of different nuclear spin symmetries. This pioneer work, although strictly empirical, proposed the first self sufficient set of parameters for absorption calculations accounting for line mixing. Very recently, Benner *et al.*[11] further extended their multispectrum fitting technique by including line mixing using the full relaxation operator; the resulting approach has the advantage of remaining valid at pressures where the Rosenkranz approximation breaks down. A very large work was carried out,[11] in which over 40 spectra of the self- and air-broadened ν_3 band were treated, fitting some diagonal and off-diagonal elements of the relaxation matrix. This study confirms that mixing between states of different nuclear spin symmetry is negligible and brings interesting indications on some possible collisional selection rules, which are discussed in this paper. Again, this approach is strictly empirical but it leads to very good agreement with measured data and, contrary to the first order development, it is not limited to low pressures.

The present paper is, to our knowledge, the first in which a comprehensive theoretical approach is proposed for line-mixing effects in infrared bands of methane. New measurements have been made in the ν_3 band of CH_4-N_2 mixtures at room temperature. These include low pressure ($\leqslant 2$ atm) experiments quite similar to those of Refs. 9, 11 and more original measurements at elevated density (>25 atm). In the model proposed, the off-diagonal elements of the relaxation matrix, which account for line coupling, are constructed starting from state-to-state rotational transfer rates. The latter are computed from the intermolecular interaction potential energy surface by using a semiclassical model.[12] Connection between state-to-state data and the line-mixing coefficients is made by introducing two empirical parameters whose values are determined by a fit of a single high pressure spectrum. Comparisons of computed results with the numerous other laboratory measurements demonstrate the quality of the model under conditions where the influence of line mixing on the absorption shape is large. In particular, the evolution of the absorption shape with the pressure and rotational quantum number J are correctly predicted. Some discrepan-

cies which appear for high J R lines are discussed. The remainder of the paper is organized as follows: the laboratory experiments are described in Sec. II. Sections III and IV present the model and the data used. Comparison between computed and recorded spectra are discussed in Sec. V.

II. EXPERIMENT

Measurements of absorption by CH_4-N_2 mixtures have been made at room temperature by the groups and instruments listed in Table I where the experimental conditions are summarized. A large pressure range has been covered, including two series for ''high'' (25–80 atm) and ''low'' (0.25–2.0 atm) pressures, respectively. The first set is characterized by the fact that the lines inside each cluster (Q branch and manifolds) strongly overlap and merge into a smooth envelop; the fine spectral structure is then masked by the influence of collisions. The spectra show strong line-mixing effects but bring no detailed information on what happens inside the merged absorption features. On the other hand, most of the fine structure remains discernible in the low pressure measurements. This provides precious additional information and a further test of the model although modifications induced by line mixing are less spectacular than at elevated pressure. Since all studied gas samples contain small mixing ratios of methane, the contribution of CH_4-CH_4 interactions is negligible. Pressure normalized absorption (α/P_{CH_4} in cm^{-1}/atm) is thus presented and the theoretical analysis only accounts for CH_4-N_2 collisions. Finally, note that the low pressure FT and TDFS spectra are in good agreement and that the measurements made in Madrid are similar to those of Ref. 9 but extend the pressure (up to 2 atm) and rotational quantum number (up to $J=16$) ranges. Note that measured spectra were corrected in order to get rid of possible errors in the line intensities and of uncertainties on the partial pressures of methane used. This was done as in Ref. 13 by multiplying experimental results by a constant factor such that the measured and computed values of integrated absorption match.

A. High pressure FT spectra in Orsay

The high pressure experiments have been carried at the LPMA in Orsay, with a Bruker IFS66V Fourier transform spectrometer. The entire ν_3 band of CH_4 perturbed by N_2 at ambient temperature was recorded with a resolution of 0.12 cm^{-1} (full-width at half-maximum) using a water cooled SiC

glow bar source. Two single pass cells of lengths 4.78 cm and 215 cm have been used, in order to study both strong and weak absorption regions. The detector is a room temperature DTGS element for internal measurements (compartment) with the short cell. A liquid nitrogen cooled InSb detector was used for the external measurements with the long cell. The pressures above 5 atm were measured with several adapted piezoresistive pressure transducers. Low pressure measurements were performed by using capacitive diaphragm type pressure transducers designed for 0–10, 0–100, and 1–1000 Torr ranges. High purity CH_4 (>99.9995%) and N_2 (>99.9999%) gases were used without further purification. Very small relative amounts of CH_4 have been used (see Table I) and spectra were recorded about $\frac{1}{2}$ h after introducing the gases in the cell. This insured a good mixing of the components that was successfully checked by comparing different spectra.

In order to achieve good accuracy on absorption coefficients in a wide range, transmission spectra with different CH_4 partial pressure were recorded for each value of the total pressure. For each spectrum, we extracted the relevant information in the spectral window when the transmission was between 0.2 and 0.8, and we reconstructed the ''whole'' ν_3 band absorption coefficient for the three total pressures (25, 50, and 80 atm).

B. Low pressure FT spectra in Paris

Nitrogen broadened spectra of methane have been recorded with the Fourier transform spectrometer built at the LPMA in Paris.[14] The White cell has a one meter baselength and was filled with binary gas mixtures at pressures of about 0.5 and 1 atm. Experiments were made with CH_4 pressures between about 0.03 and 6 Torr using path lengths of 4 and 20 m. This provided low optical thickness measurements for the study of the central absorption shape as well as optically thick media for the study of the wings. The lowest CH_4 partial pressures have been performed using for the fillings of the White cell a preliminary diluted sample by N_2 with a CH_4 concentration of 5%. A Datametrics pressure transducer has been used for the measurements below 10 Torr with an accuracy in order of 0.5%; while, for the total pressure measurements, a Texas Instrument Bourdon gauge with one atmosphere range has been employed giving an absolute accuracy of 0.03 Torr. A maximum optical path difference giving a response function width at least three times narrower than the absorption lines has been used to optimize the signal to noise ratio and the distortion effect of the spectrometer resolution. The studied spectral range is delimited by an optical filter in front of the InSb detector and extends from 2400 cm^{-1} to 3700 cm^{-1}. Before each record, an empty cell spectrum allows to compensate the variation of the incident intensity coming from the source and detector efficiencies and residual channeling.

C. Low pressure TDFS spectra in Madrid

Spectra of the $R(8)$, $R(10)$, $R(12)$, $R(14)$, and $R(16)$ manifolds have been recorded with the tunable difference frequency spectrometer at the IEM in Madrid.[15,16] About 1

μW of cw tunable IR radiation is generated by difference frequency mixing, in a $LiNbO_3$ crystal, the outputs of an Ar^+ laser (single mode, tuned to the 488 nm line), actively frequency stabilized and locked to a $^{130}Te_2$ sub-Doppler transition,[17] and of a ring dye laser operated with rhodamine 6G. The internal precision of the frequency scale and the instrumental resolution are both $\sim 10^{-4}$ cm^{-1}. The infrared beam was splitted into two paths (one traveling through the cell to an InSb detector and the other traveling in the air to another InSb detector) and the signals ratioed out to compensate unwanted IR power fluctuations. The stainless steel cell used had 645 mm pathlength and was fitted with CaF_2 wedges. Pressures were read with a capacitance manometer designed for the 0.1–1330 mbar range, with a resolution of 0.1 mbar and an accuracy of 0.5% of the reading. The pressure gauge was mounted on the cell body to continuously monitor any possible pressure evolution, except for the 2 atm measurements that were out of gauge range. In these cases the pressure was measured after the recording of the spectrum by expanding the cell content into a calibrated volume. The gases were supplied by Air Liquide and used without further purification (nominal purities were CH_4: 99.95%, N_2: 99.995%). The mixtures at 10 atm pressure were prepared in sample cylinders at least one day before the experiments with approximately 0.04 to 1.8% of CH_4 in N_2, depending on the maximum absorption intensity of each manifold.

Measurements were made as follows: an empty cell spectrum was recorded first, then the gas mixture was added up to the highest pressure to be measured and subsequent spectra recorded pumping out part of the mixture, in a nominal sequence of 2000, 1000, 500, 250 mbar. Another empty cell spectrum was finally recorded. All spectral traces are frequency linearized, calibrated and ratioed against an average of the empty cell spectra. Frequency scale linearization is done by interpolation between the frequency markers produced by a confocal Fabry–Perot interferometer (finesse 150, free spectral range 0.004 998 5(2) cm^{-1}) in a fraction of the ring dye laser.

III. THEORETICAL MODEL

A. Absorption coefficient

Consider a mixture of CH_4 in N_2 (collision partner, infrared inactive), of respective partial pressures P_{CH_4} and P_{N_2} ($P_{CH_4} \ll P_{N_2}$) at temperature T. Within the impact and binary collisions formulation of the spectral shape, the absorption coefficient α in the infrared region studied here, accounting for line mixing at wave number σ is given by[18,19] [Note, that in the correct expression a hyperbolic tangent and the sum of the lower and upper states populations appear. The terms in Eq. (1) should then be multiplied by $(1 + e^{-hc\sigma_k/k_BT})/(1 + e^{-hc\sigma/k_BT})$ but this correction is negligible in the mid-infrared region studied here.]

$$\alpha^{LM}(\sigma, P_{CH_4}, P_{N_2}, T)$$

$$= \frac{8\pi^2 \sigma}{3hc} [1 - \exp(-hc\sigma/k_B T)]$$

$$\times P_{CH_4} \text{Im} \left\{ \sum_k \sum_{k'} \rho_k(T) d_k d_{k'} \right.$$

$$\left. \times \langle\langle k' | [\Sigma - \mathbf{L_0} - iP_{N_2}\mathbf{W}(T)]^{-1} | k \rangle\rangle \right\}. \quad (1)$$

The sums in Eq. (1) include all absorption lines k and k', and Im$\{\cdots\}$ denotes the imaginary part. ρ_k and d_k are, respectively, the fractional population of the initial level of line k and the dipole transition moment. Σ, $\mathbf{L_0}$, and $\mathbf{W}$ are operators in the (Liouville) line space. The first two are diagonal, associated with the scanning wavenumber σ and with the positions σ_k of the unperturbed lines, i.e.,

$$\langle\langle k' | \Sigma | k \rangle\rangle = \sigma \times \delta_{k,k'}, \quad \langle\langle k' | \mathbf{L_0} | k \rangle\rangle = \sigma_k \times \delta_{k,k'}. \quad (2)$$

The relaxation operator $\mathbf{W}$ contains all the influence of collisions on the spectral shape. It depends on the band, on the temperature, and on the collision partner. Its off-diagonal elements account for interference between absorption lines, whereas the diagonal terms are the pressure-broadening (γ_k) and -shifting (δ_k) coefficients of the isolated lines, i.e.,

$$\langle\langle k | \mathbf{W}(T) | k \rangle\rangle = \gamma_k(T) - i\delta_k(T). \quad (3)$$

When line mixing is disregarded, the off-diagonal elements of $\mathbf{W}$ are neglected and Eq. (1) reduces to the addition of Lorentzian line contributions, i.e.,

$$\alpha^{No\,LM}(\sigma, P_{CH_4}, P_{N_2}, T)$$

$$= \sigma[1 - \exp(-hc\sigma/k_B T)] \times P_{CH_4}$$

$$\times \sum_k \frac{S_k(T)}{\sigma_k[1 - \exp(-hc\sigma_k/k_B T)]} \times \frac{1}{\pi}$$

$$\times \frac{P_{N_2}\gamma_k(T)}{[\sigma - \sigma_k - P_{N_2}\delta_k(T)]^2 + [P_{N_2}\gamma_k(T)]^2}, \quad (4)$$

where the integrated intensity S_k of line k is given by

$$S_k(T) = \frac{8\pi^3}{3hc} \sigma_k[1 - \exp(-hc\sigma_k/k_B T)]\rho_k(T) d_k^2. \quad (5)$$

B. Relaxation operator

In the present work, the real part of the off-diagonal elements of $\mathbf{W}$ is constructed starting from state-to-state collisional rates. This is not straightforward since the latter involve two quantum states only whereas the line-coupling terms depend on four (lower and upper levels of the k and k' lines). In order to connect both quantities, empirical factors are generally introduced (e.g., in N_2O,[20] CO_2,[20,21] O_3,[22]...) which somehow account for the influence of the types (P,Q,R) of the lines considered. Within this approach, the real element of the relaxation operator coupling lines k and k' is given by

$$\text{Re}\{\langle\langle k' | \mathbf{W}(T) | k \rangle\rangle\} = -A(k',k) \times K_{ik' \leftarrow ik}(T)$$

$$(\text{for } k \neq k'), \quad (6)$$

where $K_{ik' \leftarrow ik}(T)$ is the collisional transfer rate from the lower level ik of line k to the lower level ik' of line k'. Note that these parameters, as the elements of $\mathbf{W}$, satisfy the detailed balance principle and some selection rules (e.g., no collisional transfer between states of different nuclear spin). The parameters $A(k',k)$ introduced in Eq. (6) connect the state-to-state rates to the off-diagonal $\mathbf{W}$ matrix elements. In order to simplify the problem, three steps are used; (i) we first make the approximation that $A(k',k)$ depends on the branches (i.e., P, Q, or R) to which k and k' belong but not on the quantum numbers of the lines themselves. At this step, there are nine parameters left, [$A(X,Y)$, with $X,Y = P, Q,$ or R] which take into account the fact that, for given initial states, line coupling depends on the branches to which the considered optical transitions belong. (ii) The second approximation is reasonable considering obvious symmetries of the problem. It simply assumes the following equalities:

$$A(R,R) = A(P,P),$$

$$A(Q,R) = A(R,Q) = A(P,Q) = A(Q,P), \quad (7)$$

$$A(R,P) = A(P,R),$$

that reduce the number of parameters to four [$A(R,R)$, $A(R,Q)$, $A(R,P)$, and $A(Q,Q)$, for instance]. (iii) Finally one can get rid of the interbranch parameters $A(Q,R)$ and $A(R,P)$ by using the fundamental sum rule,[23]

$$\gamma_k(T) = -\sum_{k' \neq k} \frac{d_{k'}}{d_k} \text{Re}\{\langle\langle k' | \mathbf{W}(T) | k \rangle\rangle\}, \quad (8)$$

which directly translates to

$$\sum_k \rho_k(T) d_k^2 \times \gamma_k(T) = \sum_k \sum_{k' \neq k} \rho_k(T) d_k d_{k'} \times A(k',k)$$

$$\times K_{ik' \leftarrow ik}(T). \quad (9)$$

Restricting the sum over k to lines of the Q branch only leads to a relation between $A(R,Q) = A(P,Q)$ and $A(Q,Q)$. Then applying the same equation to lines k of the P branch relates $A(R,P)$ to $A(P,P) = A(R,R)$ and $A(Q,P) = A(Q,R)$. Once the state-to-state rates and broadening coefficients are known, the model is thus based on two parameters only [$A(R,R)$ and $A(Q,Q)$ have been retained here]. They are empirical and need to be determined from fits of measured spectra as done in Sec. IV. Note that they do not depend on the considered lines and that the same values are used for all transitions and pressures.

The construction of the off-diagonal imaginary part of $\mathbf{W}$ from theory is an intractable problem and Im$\{\mathbf{W}\}$ was restricted to its diagonal part (line shifts). This approximation is likely sufficient considering the pressure range studied and the fact that the off-diagonal terms are expected to be small.

J. Chem. Phys., Vol. 110, No. 16, 22 April 1999

Pieroni *et al.* 7721

C. State-to-state collisional rates

The semiclassical model used for line broadening in Refs. 4, 12, 24, 25, was applied to the calculation of relaxation rate constants for CH_4–Ar. (The use of CH_4–Ar state-to-state rates to model the effect of CH_4–N_2 collisions on the spectral shape is discussed in Appendix A.) Various modification and improvements of the calculations described in Ref. 12 have been implemented as described in Ref. 26. The main points of the model are recalled below.

Several studies (see Refs. 27–37) have been devoted to the methane–rare gas interaction potential surface, which is the starting point of the calculation. In the present work, a Lennard-Jones-type atom–atom potential was used as described in Ref. 24. Its tensorial expression is

$$V^{\text{at–at}}(R,\Omega_1) = \sum_{\substack{l_1=0,3,4,6 \\ q=l_1,l_1+2,\dots}} \left[d_q^{l_1\Gamma_1} \frac{D_q^{l_1\Gamma_1}}{R^{12+q}} - e_q^{l_1\Gamma_1} \frac{E_q^{l_1\Gamma_1}}{R^{6+q}} \right] \times D_0^{(l_{1g},l_{1g}\Gamma_1)}, \tag{10}$$

where R is the center-of-mass separation between the XY_4 molecule and the atom. Ω_1 represents the three Euler angles giving the orientation of the XY_4-fixed frame with respect to a frame whose z axis is along the intermolecular axis. The $d^{\cdots}$ and $e^{\cdots}$ are numerical coefficients. The $D^{\cdots}$ and $E^{\cdots}$ are polynomials of the atom–atom Lennard-Jones parameters. The $D^{\cdots}$ are symmetrized angular operators whose expressions are given in Ref. 24. Γ_1 is the symmetry in the T_d group of a given operator. $\Gamma_1 = A_1$ for $l_1 = 0$, 4 or 6, and $\Gamma_1 = A_2$ for $l_1 = 3$. The order of development for radial parts and angular operators as well as the values for the four atom–atom parameters are the same as in Refs. 12, 25 for the methane–argon system.

Starting from knowledge of the CH_4–Ar interaction, the calculations were done at room temperature. As developed in Ref. 12, the rotational energy relaxation rate constant (in units of cm^{-1}/atm) from quantum state i to state j is given by

$$K_{j\leftarrow i} = \frac{n\bar{v}}{2\pi c} \int_{r_{c_0}}^{\infty} dr_c r_c \left(\frac{v_c'}{\bar{v}} \right)^2 S_{2,i\rightarrow j}'(r_c,\bar{v}). \tag{11}$$

In this expression, n is the density of collision partners for 1 atm at the considered temperature and $\bar{v}$ is the mean relative velocity. r_{c_0} is the distance of closest approach and v_c' is the apparent velocity on the equivalent straight line trajectory. $S_{2,i\rightarrow j}'(r_c,\bar{v})$ is the renormalized second order collision probability (see below). In Ref. 12 calculations were done at one single velocity (the mean thermal velocity). Nevertheless, it seems more realistic to take into account the effect of the change in internal energy which is gained or lost by the relative translational degrees of freedom. For the present calculations, the velocity at infinite impact parameter was thus set to depend on the particular couple of states under consideration. This was done by replacing the mean thermal velocity by an effective velocity defined by

$$v_{i\rightarrow j}^{\text{eff}} = \frac{v_{\text{initial}} + v_{\text{final}}}{2} = \frac{\bar{v}}{2} \left[1 + \left(1 - \frac{\Delta E_{i\rightarrow j}}{\mu\bar{v}^2/2} \right)^{1/2} \right], \tag{12}$$

where μ is the reduced mass and $\Delta E_{i\rightarrow j} = E_j - E_i$ is the energy involved in the considered rotational transfer. Since this modification can lead to unrealistic results for large positive values of $\Delta E_{i\rightarrow j}$, Eq. (12) was applied to downward collisions only and upward transitions were deduced from the detailed balance relationship $[\rho_i K_{j\leftarrow i} = \rho_j K_{i\leftarrow j}]$.

One important problem in semiclassical calculations is that the S_2 function can take values larger than one for small impact parameters. Although this problem may be partly avoided through the parabolic trajectory model, it is more correct to introduce a normalization condition for the matrix elements of the diffusion operator. We used the procedure introduced in Ref. 38, and first set

$$S_{2,i}(r_c,\bar{v}) = \sum_{j\neq i} S_{2,i\rightarrow j}(r_c,\bar{v}), \tag{13}$$

where $S_{2,i\rightarrow j}$ is defined as in Ref. 12 (i.e., without any renormalization condition). Then we define

$$\bar{S}_{2,i\rightarrow j}(r_c,\bar{v}) = S_{2,i\rightarrow j}(r_c,\bar{v}), \quad \text{if } S_{2,i\rightarrow j}(r_c,\bar{v}) \leq 1,$$
$$\bar{S}_{2,i\rightarrow j}(r_c,\bar{v}) = 1, \quad \text{if } S_{2,i\rightarrow j}(r_c,\bar{v}) \geq 1. \tag{14}$$

Using these new probabilities, one can define

$$\bar{S}_{2,i}(r_c,\bar{v}) = \sum_j \bar{S}_{2,i\rightarrow j}(r_c,\bar{v}). \tag{15}$$

The renormalized probabilities used in Eq. (11) are then given by

$$S_{2,i\rightarrow j}'(r_c,\bar{v}) = \frac{\bar{S}_{2,i\rightarrow j}(r_c,\bar{v})}{\bar{S}_{2,i}(r_c,\bar{v})} [1 - \exp(S_{2,i}(r_c,\bar{v}))]. \tag{16}$$

The limitations of calculations of state-to-state rates with the present approach have been discussed previously.[12,38] Among these is the fact that the semiclassical approach fails down when large internal energy changes are considered; this limits application of the model to states for which $|\Delta E_{i\rightarrow j}|$ is small when compared with kinetic energy (i.e., $\approx k_B T$). Hence results for $\Delta J \neq 0$ transfers between high rotational quantum number J levels are likely inaccurate. Fortunately, the states associated with lines within a given P or R manifold practically have the same energy so that only quasiresonant collisions are involved. An other limitation is due to the use of limited expansions of the potential and of the diffusion operator. As a results some transfers are missing in the model and this affects all results through the renormalization procedure. For instance, the $\Delta J = 3$ rates computed with the present approach result from the single "jump" associated with the potential matrix element $\langle J+3|V|J\rangle$; they do not include contributions associated with higher order terms in the expansion of the diffusion operator (such as $\langle J+3|V|J+1\rangle \times \langle J+1|V|J\rangle$ or $\langle J+3|V|J+2\rangle \times \langle J+2|V|J+1\rangle \times \langle J+1|V|J\rangle$). Hence one expects that the present approach correctly predicts only the main channels, that have the largest rates and involve reasonable changes in internal energy and quantum numbers.

IV. DATA USED

The data required for computations using Eq. (1) are the position σ_k, population ρ_k, and dipole matrix element d_k of each line k, and elements of the relaxation operator.

In the present work, all the σ_k, ρ_k, and d_k parameters have been taken from the 1996 version of the HITRAN database.[39]

Values of the diagonal elements of **W** (half-widths γ_k and shift δ_k of the lines) for CH_4–N_2 have been determined as follow: a first set was constructed, for all lines centered in the spectral range studied, by multiplying the CH_4–air values of HITRAN by the factor 1.02.[6,40] When possible, the values for the ν_3 band lines of $^{12}CH_4$ were then replaced by measured data. This was done using the experimental results of Refs. 6, 9, and 40, privileging the more recent data provided by Pine.[9]

Only the real part of the off-diagonal elements of **W** was considered and coupling was restricted to the ν_3 band of $^{12}CH_4$. Hence the contributions of all the other lines ($^{13}CH_4$, hot and combination bands,...) were computed neglecting line mixing, through the addition of Lorentzian (Voigt) profiles. Fortunately, this approximation has little consequences on computed results since absorption in the studied region is largely dominated by the contribution of the ν_3 band. Within these approximations, the $\mathrm{Re}\{\langle\langle k'|\mathbf{W}(T)|k\rangle\rangle\}$ terms were calculated, up to $J=17$ (≈ 400 lines) using Eq. (6) and state-to-state rates calculated as described in Sec. III C. The values of $A(R,R)$ and $A(Q,Q)$ were determined as explained below and the other $A(X,Y)$ parameters were deduced from Eqs. (7) and (9). Note that the use of cross sections for CH_4–Ar in order to model CH_4–N_2 spectra is discussed in Appendix A and that selection rules are the subject of Appendix B.

In order to adjust the $A(R,R)$ and $A(Q,Q)$ empirical constants, the 25 atm spectrum has been used. Least squares fits of measured absorption in the Q branch region and the $R(8)$ manifold were made with the model and data described above. The choice of the particular $R(8)$ manifold results from three reasons; the first is that the R branch is more adapted for the determination of $A(R,R)=A(P,P)$; indeed, ν_3 lines within the manifolds are more closely spaced and less contaminated by transitions of other bands in the R branch than in the P branch. The second point is that important line-mixing effects (and thus high sensitivity to A) occur for high rotational quantum numbers. Increased accuracy on $A(R,R)$ is thus expected from the use of high J manifolds. The last reason is that the retrieved value is clearly dependent on the line-broadening and -shifting parameters used in the calculation. The latter must be reliable and this constraint practically restricts the choice to the lines studied in Ref. 9. For all these reasons the $R(8)$ manifold is a good compromise and was retained for the fit of the $A(R,R)$ constant. The final parameters are $A(R,R)=0.58$ and $A(Q,Q)=0.30$. Through Eq. (9) they lead to $A(Q,R)=0.47$ and $A(P,R)\approx 0$ and the other parameters are given by Eq. (7). Note that these values connect state to state rates to line mixing parameters but also include the change from CH_4–Ar to CH_4–N_2 collisions. Figures 1 and 2 show the quality of the fit. Values calculated using purely Lorentzian line shapes have also been plotted, that indicate the important effect of line mix-
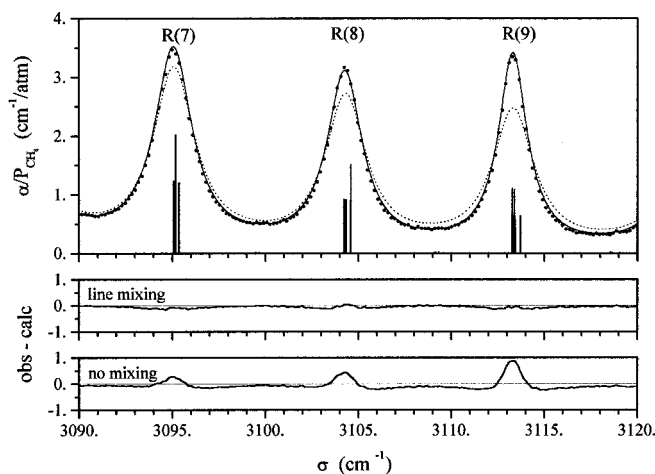

FIG. 1. Absorption in the $R(7)$–$R(9)$ manifolds for the pressure of 24.4 atm. ● are measured values, whereas — and --- have been calculated with and without the inclusion of line mixing, respectively. Obs−calc deviations are given in the lower part of the plot and the spectral line structure is indicated by the vertical bars.

ing; as is now well known, the collisional transfers between optical transitions lead to a narrowing of the spectral shape. Note in Fig. 1 that the profiles of the $R(7)$ and $R(9)$ manifolds, not used in the fit, are correctly predicted by the model.

V. RESULTS AND DISCUSSION

The laboratory spectra at our disposal, recorded by the experimental groups listed in Table I, are used in order to assess the quality of the theoretical approach. The large variety of pressure conditions (from 0.25 to 80 atm) provides an extensive test of the model. Comparisons are made between measured values and results computed with and without the inclusion of line mixing.

A. High pressure absorption

Figures 3 and 4 present results obtained in the P and R branches of the ν_3 band for a total pressure of 50 atm and values of the initial level quantum number J between 5 and
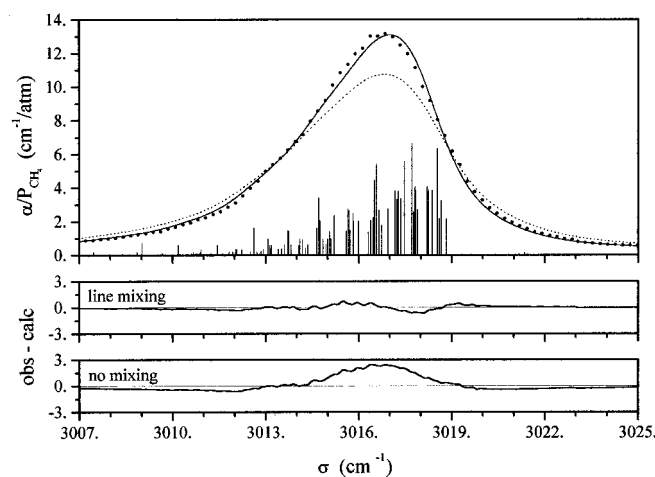

FIG. 2. Absorption in the Q branch for the pressure 24.4 atm. Same legend and symbols as in Fig. 1.
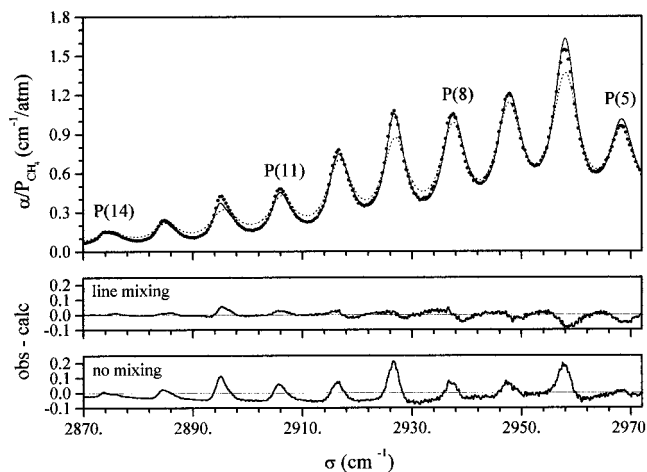
FIG. 3. Absorption in the *P* branch for the pressure 49.0 atm. Same legend and symbols as in Fig. 1.

FIG. 5. Absorption in the ν_3 band for the pressure 49.0 atm. Measured values are plotted in the upper part. (Obs−calc)/obs relative deviations are displayed in the lower part where — and --- have been calculated with and without the inclusion of line mixing, respectively.

15. These plots confirm that neglecting line mixing leads to large errors and that our model gives satisfactory predictions. Note that our approach leads to almost perfect results for the manifolds where accurate measured line-broadening data were available and could be used. This is particularly clear in the *R* branch (Fig. 4) where the quality of the model breaks down above $J \approx 10$ which is the highest value studied in Ref. 9. For $J > 10$, we had to use the HITRAN values of γ_k and δ_k. The fact that the quality of these parameters is questionable for transitions where no measurements have been made seems a possible explanation of the increase of discrepancies between measured and computed absorption. Indeed, the number quantifying the precision of these data given in HITRAN for these lines is 2 which corresponds to ''average of estimated value''; the broadening coefficients of high *J* *R*(*J*) lines have been set to average values[41] with very approximate dependence on quantum numbers. Line-mixing effects are underestimated, likely due, in part, to the use of overestimated values of the line broadening parameters as will be confirmed latter. Note that this does not explain the results for *R*(12) whose excessive narrowing remains unexplained
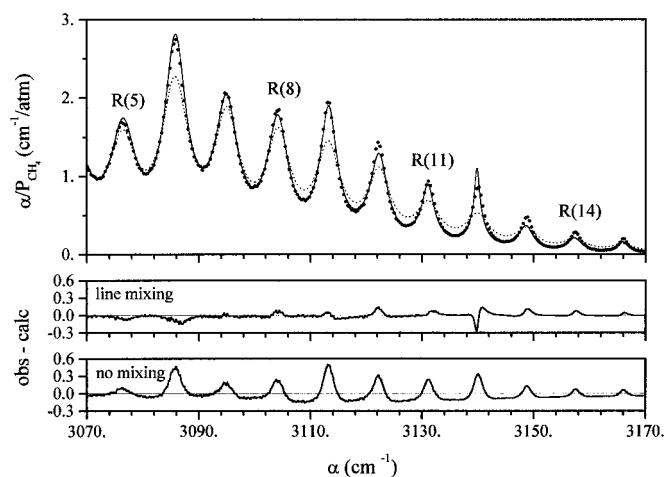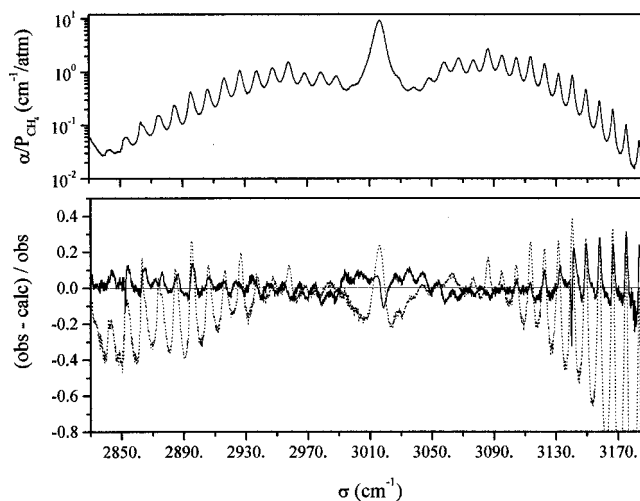
and that better results are obtained in the *P* branch, probably thanks to the measured values of γ_k given in Ref. 40. Finally, the quality of the predictions in Fig. 4 shows that assuming a constant $A(R,R)$ parameter for all *R* lines is reasonable. Furthermore, the approximation $A(P,P) = A(R,R)$ is validated by the results obtained in the *P* branch (Fig. 3). All the preceding conclusions hold for the 25, 50, and 80 atm spectra.

An overall picture of the influence of collisional transfer on the ''whole'' ν_3 band is given in Fig. 5, which shows the relative errors on the computed values. The increase, with *J*, of the errors obtained when line mixing is neglected is well evidenced. The broadening of spectral features is then overestimated leading to overestimation of absorption in the troughs and underestimation of peak values by a factor of up to 2. Note that the quality of our approach is confirmed except for the lines on the high frequency side of the band
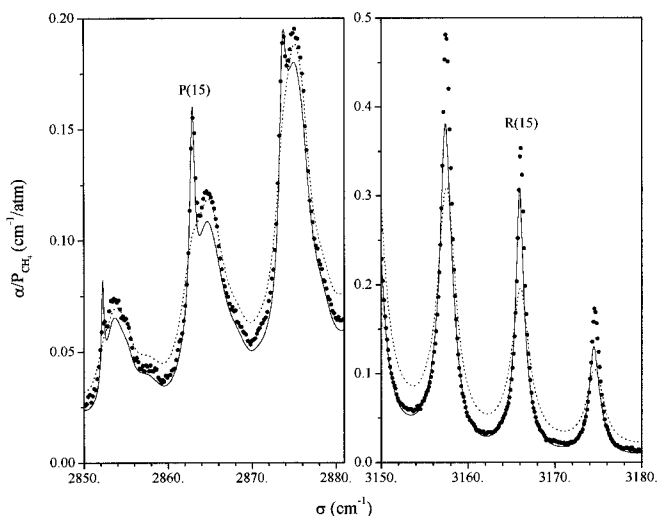

FIG. 4. Absorption in the *R* branch for the pressure 49.0 atm. Same legend and symbols as in Fig. 1.

FIG. 6. Absorption in the high *J*(14–16) *P* and *R* manifolds for the pressure 24.2 atm. ● are measured values, whereas — and --- have been calculated with and without the inclusion of line mixing, respectively.
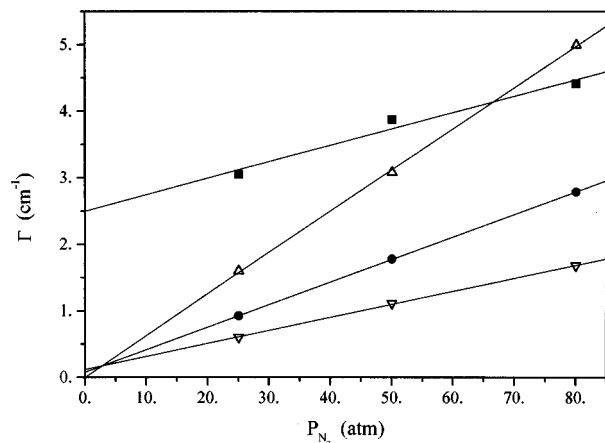
FIG. 7. Half-widths Γ of some absorption features in measured spectra vs total pressure. ■, △, ●, and ▽ have been obtained for the Q branch and the $R(5)$, $R(10)$, and $R(15)$ manifolds, respectively. The straight lines are linear fits.
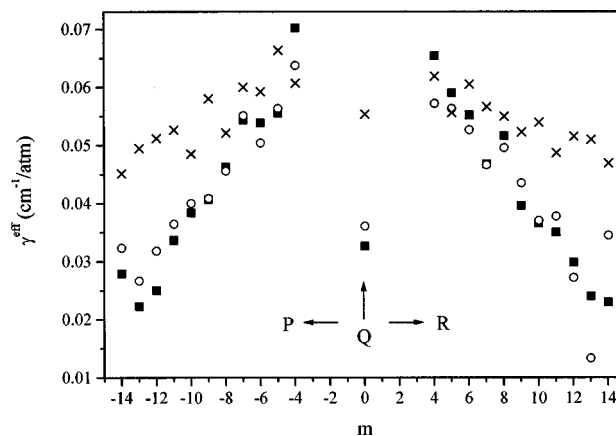

FIG. 8. Effective broadening coefficients γ^{eff} [see Eq. (17)] of the ν_3 band features. Values in the R and P manifolds are plotted vs rotational quantum number m ($-J$ and $J+1$ for P and R lines, respectively) and the results for the Q branch are given at the position $m=0$. ■ have been obtained from measured spectra; ○ and × were deduced from absorption calculated with and without the inclusion of line mixing, respectively.

($\sigma \geqslant 3120\,\text{cm}^{-1}$, $R_{J \geqslant 10}$) as is further emphasized in Fig. 6. Comparison between the measured and Lorentz profile in this plot also shows the transfer of absorption from the regions of weak absorption (troughs) to those of intense absorption (centers). It is worth noting that some particular features due to line mixing are predicted by our model: it is the case of the narrow peak on the left side of the $P(15)$ manifold, which is absent from the purely Lorentzian calculation.

For a synthetic view of the effects of collisions, we have determined the half-width at half-maximum $\Gamma(P_{N_2})$ of each absorption feature (Q branch, R and P manifolds) in the $P = 25$, 50, and 80 atm spectra. The values obtained have been fitted by the linear law

$$\Gamma(P_{N_2}) = \Delta\sigma + P_{N_2} \times \gamma^{\text{Eff}}. \tag{17}$$

The parameter $\Delta\sigma$ is representative of the spectral dispersion of the transitions that compose the considered feature; it is of the order of the intensity weighted root mean square of the line positions as suggested in Ref. 42 and confirmed by the numerical values obtained here. γ^{eff} represents the effects of collisions and is related to the relaxation operator elements by[13]

$$\gamma^{\text{eff}} = \sum_{k} \sum_{k'} \rho_k(T) d_k d_{k'} \times \text{Re}\{\langle\langle k' | \mathbf{W} | k \rangle\rangle\}, \tag{18}$$

where the sums are restricted to lines centered within the considered spectral feature. The values of Γ deduced from measured absorption in the Q branch and in the $R(5)$, $R(10)$, and $R(15)$ manifolds are plotted in Fig. 7 together with the fit using Eq. (17). It is clear from the slopes that collisions (i.e., the pressure) have effects that decrease with J. One can also check that the zero pressure intersect does represent the spectral distribution of line intensities. Values of γ^{eff} deduced from measured and computed spectra are plotted in Fig. 8, where results in the P, Q, and R branches are displayed. It is clear that the broadening coefficient of the manifold decrease with increasing J while the effects of line mixing become more and more important. When line cou-

pling is neglected, errors reach about a factor of 2. Although not perfectly, our model accounts for most of the characteristics of the influence of rotational quantum numbers on the spectral shape at high pressure. Note that the decrease of γ^{eff} results from the increasing number of states in the manifold [and in the sum in Eq. (18)], whose associated line coupling terms are quasiresonant (the lower state energies of lines within a manifold are almost equal). Analysis of the relaxation elements also shows that coupling between manifolds J and J' strongly decrease with J, J', and $\Delta J = |J - J'|$. This is expected since the associated rotational energy jump $\Delta E \approx 5\Delta J \times (J + J' + 1)\,\text{cm}^{-1}$ quickly becomes comparable with the kinetic energy [$\Delta E_{R(J+1)-R(J)} = 58$, 144, and 230 K for $J = 3$, 9, and 15, respectively]. Nevertheless, the pressures investigated in the present work are too small for significant effects of intermanifold mixing; indeed, $P \times \gamma^{\text{eff}}$ is smaller than about 3 cm^{-1}, whereas the spectral gap between adjacent manifolds is of the order of 10 cm^{-1}.

B. Low pressure absorption

As pressure decreases, collisional effects become less important and the central part of the absorption shape becomes dominated by the spectral distribution of the isolated lines.[43] On the other hand, detailed information on what happens inside the spectral structures can be brought by low pressure absorption. Indeed, it is well established that for spherical-top molecules, collisional transfer rates are extremely selective with respect to molecular symmetry species C^n (Refs. 44, 45, and references therein). In the following, the regions near the centers of P and R manifolds are considered. Results in the Q branch are not presented since the highest pressure studied (1 atm) is too low to induce large line-mixing effects (they remain lower than a few %). The influence of line mixing will then be demonstrated in the next section by considering the wings which, as is well known,[46] is affected at all pressures.

The effect of pressure on the $R(8)$ manifold is shown in Fig. 9. It is clear that the proposed model leads to better
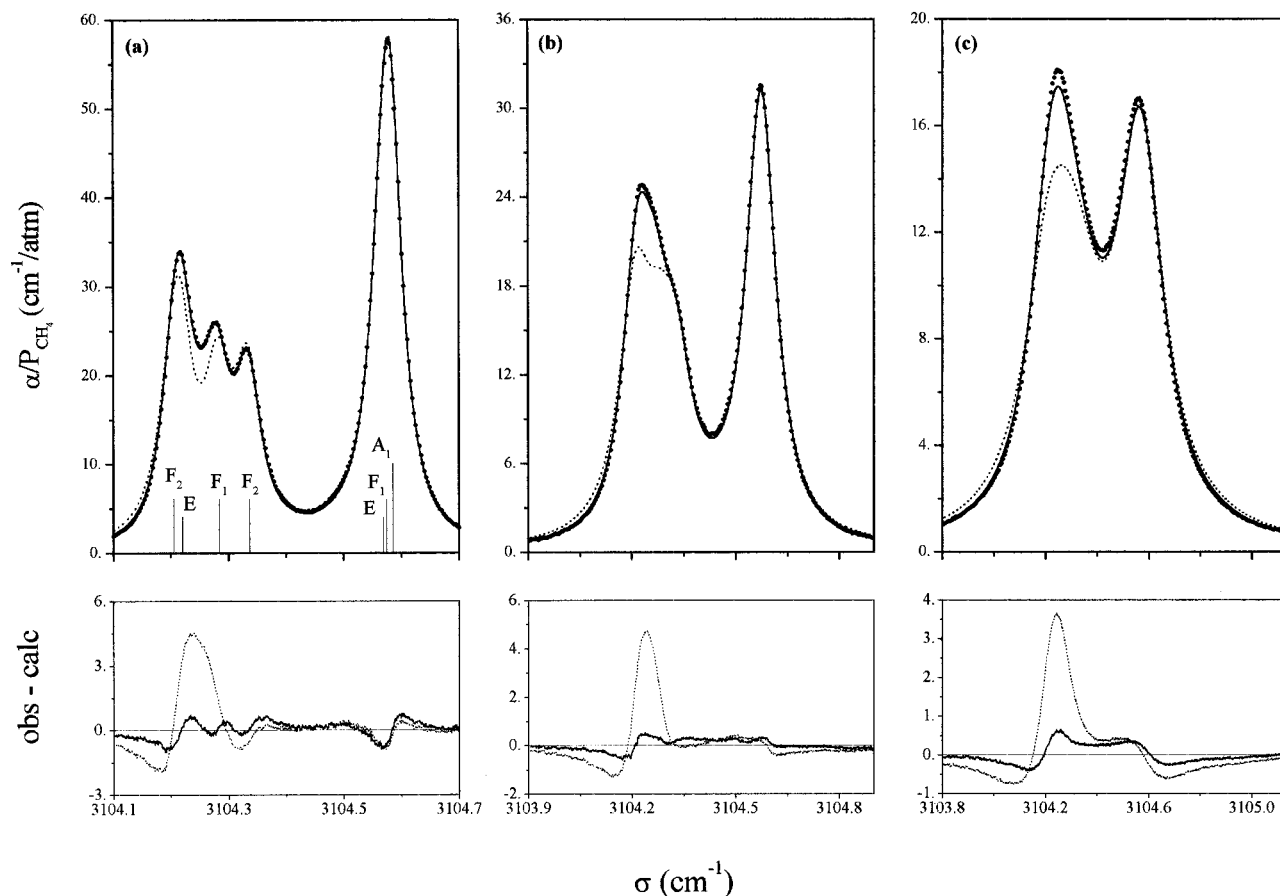
FIG. 9. Effect of pressure on the shape of the $R(8)$ manifold. ● are measured values, whereas — and --- have been calculated with and without the inclusion of line mixing, respectively. Obs−calc deviations are given in the lower part of the plot. The spectral line structure and nuclear spin symmetry of the lower levels are indicated by the vertical bars. (a), (b), and (c) are for $P_{N_2}=0.493$, 0.987, and 2.05 atm, respectively.

results than the purely Lorentzian calculation, regardless of the pressure. Note that there is no coupling between the transitions of the high frequency side which have different nuclear spin symmetries (A, E, and F) contrary to the lines on the low frequency side of the manifold where mixing between the $F_{1,2}$ components occurs. As the pressure increases, the coupled lines overlap, forming an unique cluster, which is centered at the intensity weighted average of the line positions. Its magnitude becomes higher than that of the feature on the high frequency side, contrary to what is predicted when line mixing is neglected.

Figures 10 and 11 display some P and R manifolds— where accurate values for the isolated line parameters[9] have been used for computations—giving a picture of the high selectivity of collisional processes among the tetrahedral components. Again, the main characteristics of line mixing are reproduced by our approach; the effects of the coupling between the $F_{1,2}$ (and $A_{1,2}$) components in the low frequency cluster are correctly predicted. Furthermore, our model does well account for the lack of coupling between the two F components of the high frequency cluster in the $R(7)$, $P(9)$, and $R(9)$ manifolds [Figs. 10(a), 11(a), 11(b)]. Simple fitting laws would not allow to reproduce these results, as discussed in Appendix B. The $P(9)$ and $R(9)$ manifolds [Figs. 10(a) and 11(b)] although they involve the same sequence of lower state symmetry, have quite different shapes due to differ-

ences in the rotational structure of the upper levels. In the case of the $R(9)$, the A_2, F_2, F_1, and A_1 on the left are closely spaced and collapse into a unique structure whereas only the F_2 and F_1 merge into a peak in the more sparse $P(9)$ manifold.

Results obtained for some high J lines are displayed in Fig. 12. Again, the manifolds include two clusters, that on the low frequency side being the one where line-mixing effects occur. For the high frequency feature, Lorentz and coupled calculations lead to the same results since the associated lines have different nuclear spin symmetries and thus do not mix. The broadening of these features is strongly overestimated by both models. This confirms that the line-broadening coefficients γ_k used, which are estimates provided by the HITRAN database, are too large. Note that this might also explain the fact that the narrowing of the left cluster in the $R(16)$ manifold is underestimated by our approach. On the contrary, precise values[40] were used for the mixed components of the $P(12)$ manifold where predictions of our model are satisfactory.

Remaining problems are illustrated by the spectra in Fig. 13. Again, the calculated spectral features on the right-hand sides are not affected by line mixing but are too broad. The shapes of the left clusters are improperly predicted by our line mixing model likely due to overestimation of some of the matrix elements involved. At elevated pressure (see Fig.
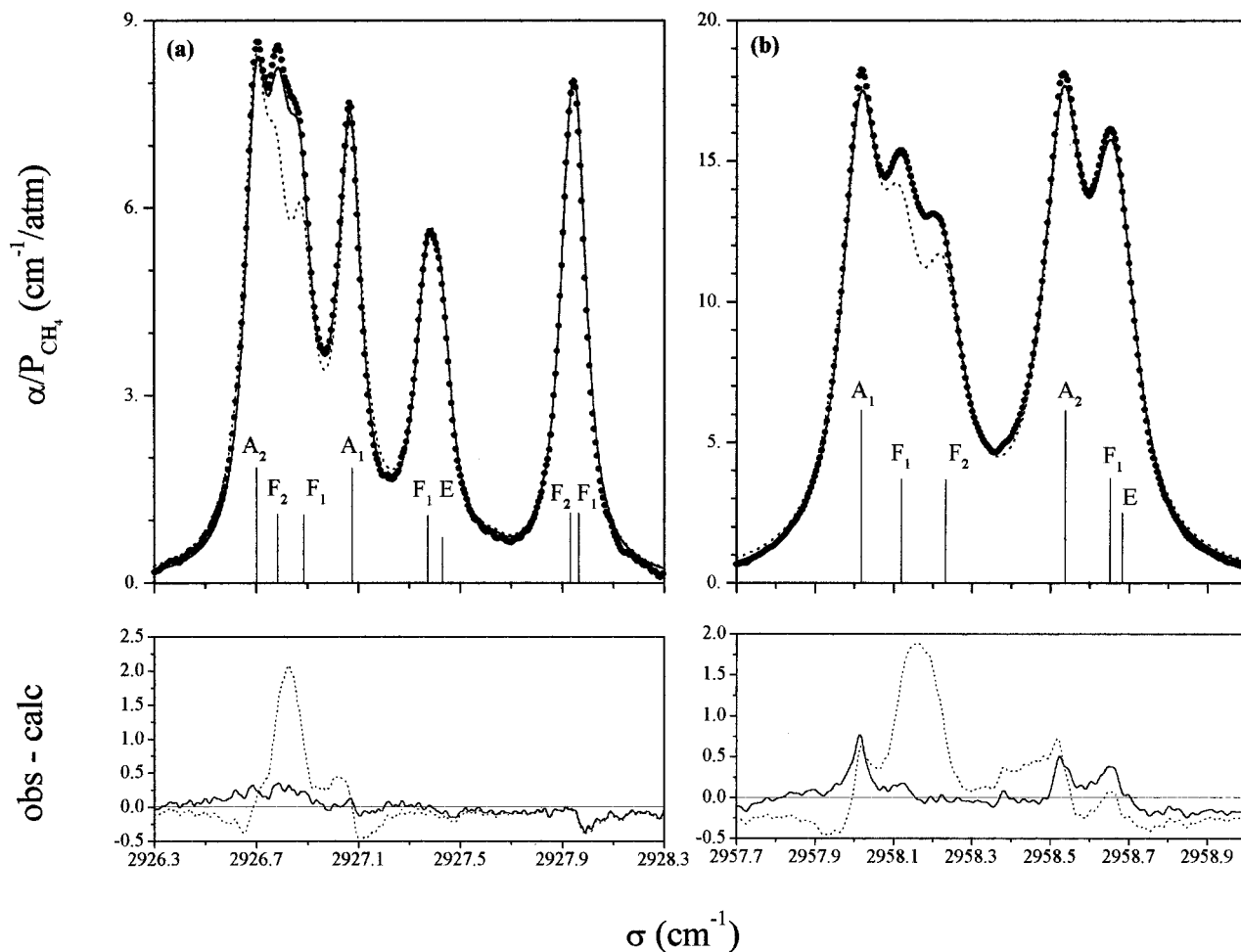
FIG. 10. Absorption in the $P(9)$ (a) and $P(6)$ (b) manifolds, for the pressure of 0.974 atm. Same legend and symbols as in Fig. 9.

3), this ''local'' effect results in overestimated narrowing of the $R(12)$; in the $R(11)$ manifold it is masked (compensated) by the overestimation of the widths of the second and third peaks in Fig. 13.

The effect of total pressure on absorption at the peak of the coupled feature in the $R(8)$ and $R(16)$ manifolds is plotted in Fig. 14. The results show the consistency between the FT and TDFS measurements and emphasize the increase of line-mixing effects with pressure and rotational quantum number. Note that, for 0.25 atm, contrary to the $R(8)$ manifold, line coupling between the $R(16)$ lines cannot be neglected, and should be accounted for in computations of stratospheric absorption. For an overall picture of the influence of line-mixing and of the quality of the models we have determined relative errors on peak absorption at $\approx$1 atm. The variations of relative errors with J, plotted in Fig. 15, again confirm the consistency of the measurements made in Paris and Madrid. The results obtained with the models are expected in view of those plotted in Fig. 8, remembering that overestimation of the broadening leads to underestimation of peak absorption (and vice versa). Neglecting line mixing leads to errors that increase with J and reach a factor of about 2. The agreement with measured values is significantly improved by using our model. The latter accounts for most

characteristics of the J dependence although, as discussed above, some problems remain.

C. Towards atmospheric transmissions

The fundamental quantities involved in atmospheric applications are the transmissions τ of the layers that compose the considered optical path. They enable computation of a number of atmospheric characteristics (emission, absorption, cooling rate, greenhouse effect,...). For a first check of the need to account for line mixing when atmospheric spectra are considered, a ''representative'' transmission spectrum was recorded in the laboratory for $P_{CH_4} = 8.2 \times 10^{-3}$ atm, $P_{N_2} = 0.985$ atm, and $L = 20.1$ m. In terms of methane absorption, these conditions are close to those of a 100 km long horizontal path at ground level. Measured and computed results are compared in Fig. 16 where details in the Q and R branch regions are plotted. The ν_3 band lines are all saturated and the narrowing due to line mixing is seen in their wings. The purely Lorentzian approach underestimates transmission whereas our approach leads to a significant improvement of the calculated values beyond the Q branch head and in-between the R manifolds. These results, and those of Sec. V B, show that great care should be taken in the determina-
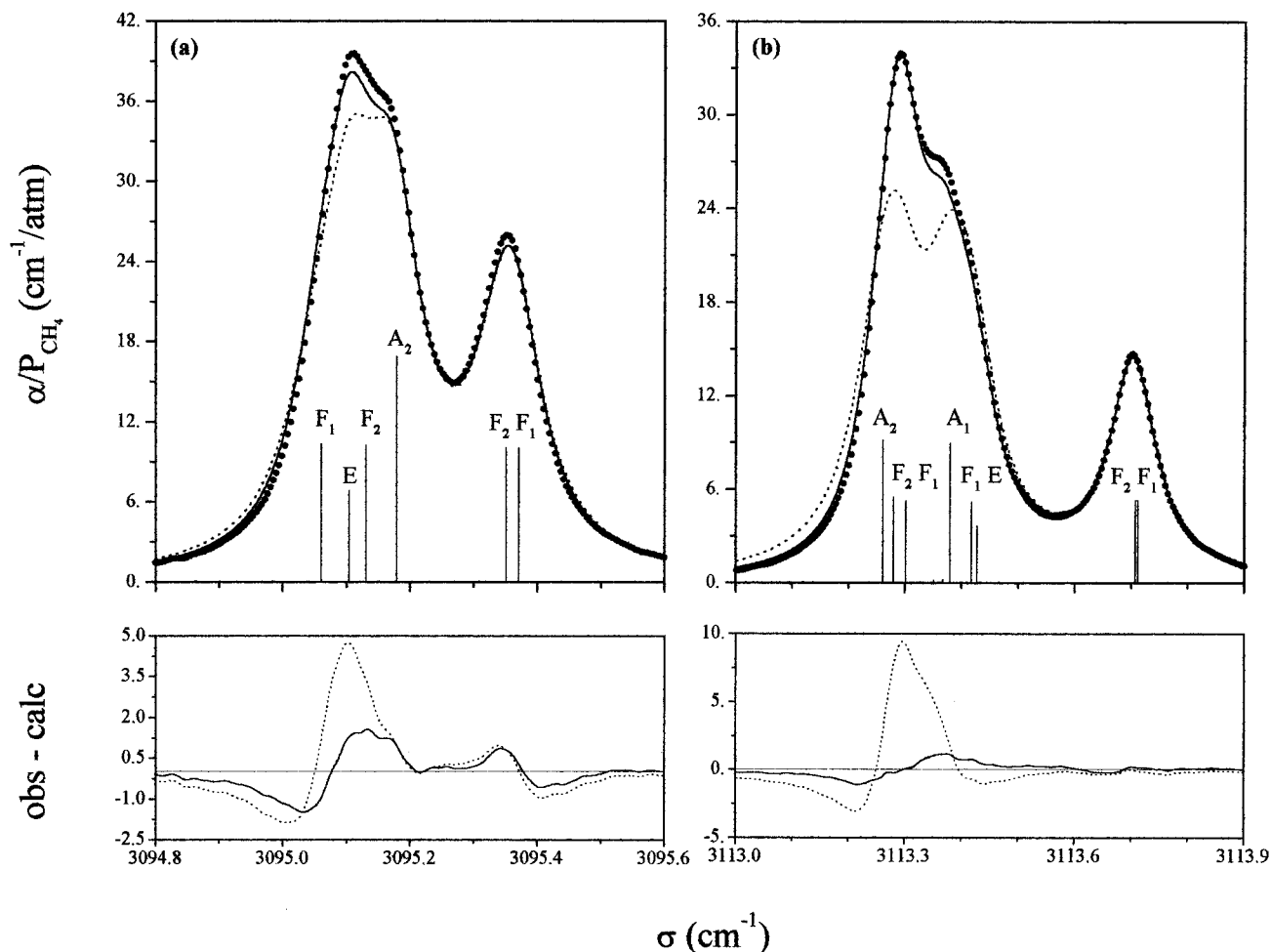
FIG. 11. Same as Fig. 10, but for the $R(7)$ (a) and $R(9)$ (b) manifolds.

tion of CH_4 mixing ratios from infrared spectra since line mixing may strongly affect the spectral feature (or its background absorption) retained for the retrieval. Furthermore, use of isolated-line models (Voigt) should be avoided for precise computations of cooling rates and greenhouse effect. Indeed, estimates of contribution of methane to the atmospheric emission and the absorption of solar radiation can be made using the spectrum of Fig. 16. These quantities, integrated over the ν_3 band are given by

Emitted intensity:

$$I_E = \int_{2800}^{3200} [1 - \tau(\sigma)] \times I_{BB}(\sigma, 300 \text{ K}) \times d\sigma,$$

Absorbed solar intensity:

$$I_A = \int_{2800}^{3200} \tau(\sigma) \times I_{BB}(\sigma, 5600 \text{ K}) \times d\sigma, \tag{19}$$

where $I_{BB}(\sigma,T)$ is the black body radiance for wave number σ and temperature T. Values of I_E and I_A have been calculated from Eq. (19) using measured and computed values of $\tau(\sigma)$. The relative errors $\Delta I = (1 - I^{\text{Calc}}/I^{\text{Exp}})$ are $\Delta I_E = -3.1\%$ and $\Delta I_A = +5.8\%$ when line mixing is neglected whereas $\Delta I_E = -0.6\%$ and $\Delta I_A = +1.5\%$ are obtained with our approach. These values confirm the need to account for

line mixing in atmospheric radiative transfer computations and demonstrate the improvement brought by our model.

VI. CONCLUSION

The model presented in this paper is based on semiclassical state-to-state rates and two empirical parameters only. It is thus, in its principle, quite different from the purely empirical approaches proposed by Pine[9] and Benner.[11] The latter lead, of course, to much better agreement with measurements and fulfill the high precision requirements of practical applications; on the other hand, they have limited predictive capabilities since they are restricted to spectral regions where proper laboratory measurements have been made and treated.

Test of our model using new high and low pressure measurements show that calculations are quite satisfactory up to rotational quantum numbers of about $J = 10$. Above this value, the main characteristics of the effects of line mixing are predicted but agreement with measurements is only qualitative, particularly in the R branch. Three main explanations stand for the increase of discrepancies with J. The first is related to the approximate nature of the state-to-state rates used here whose quality highly relies on the potential surface and the semiclassical approach. The second point is the intrinsic approximation of the model that assumes con-
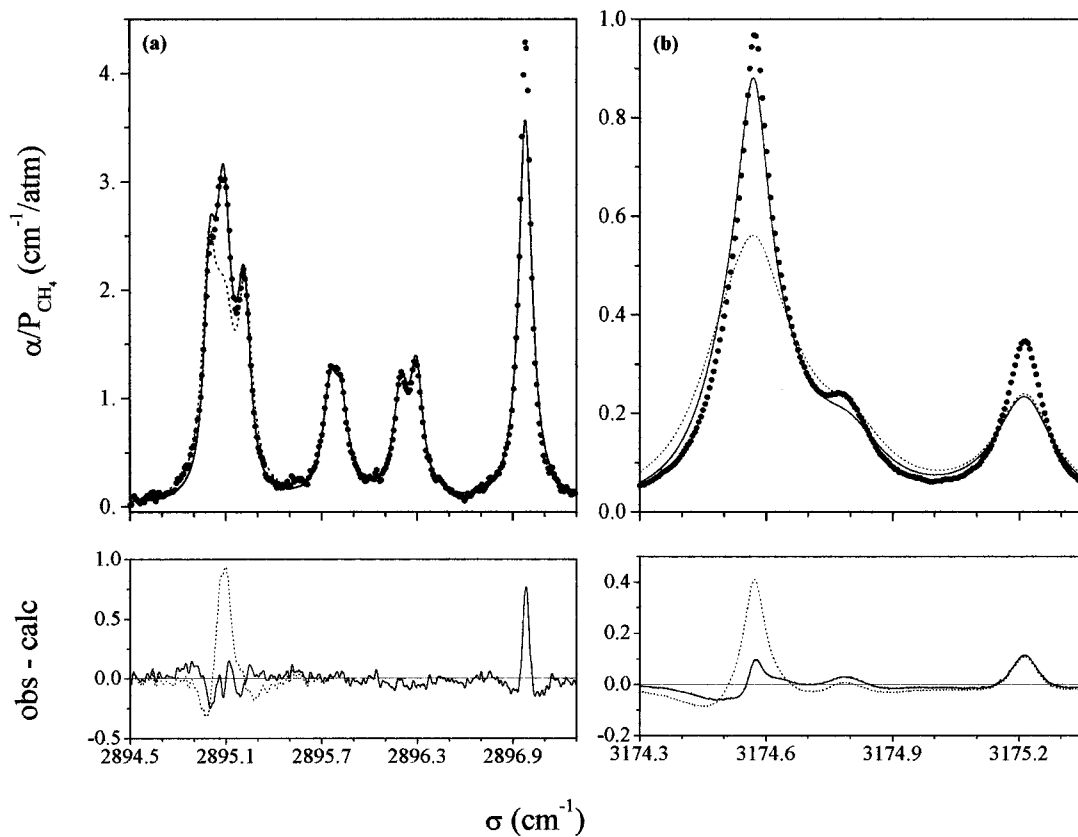
FIG. 12. Same as Fig. 10, but for the manifolds; (a) $P(12)$ at 0.973 atm; (b) $R(16)$ at 2.01 atm.
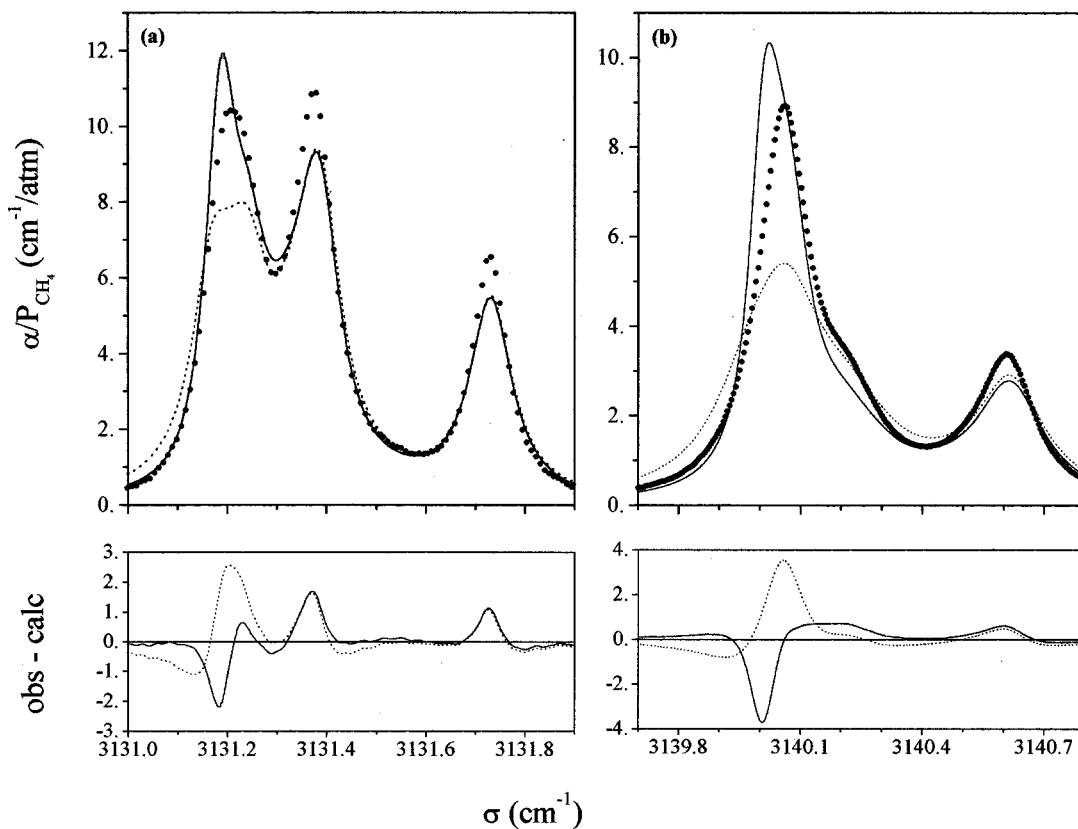

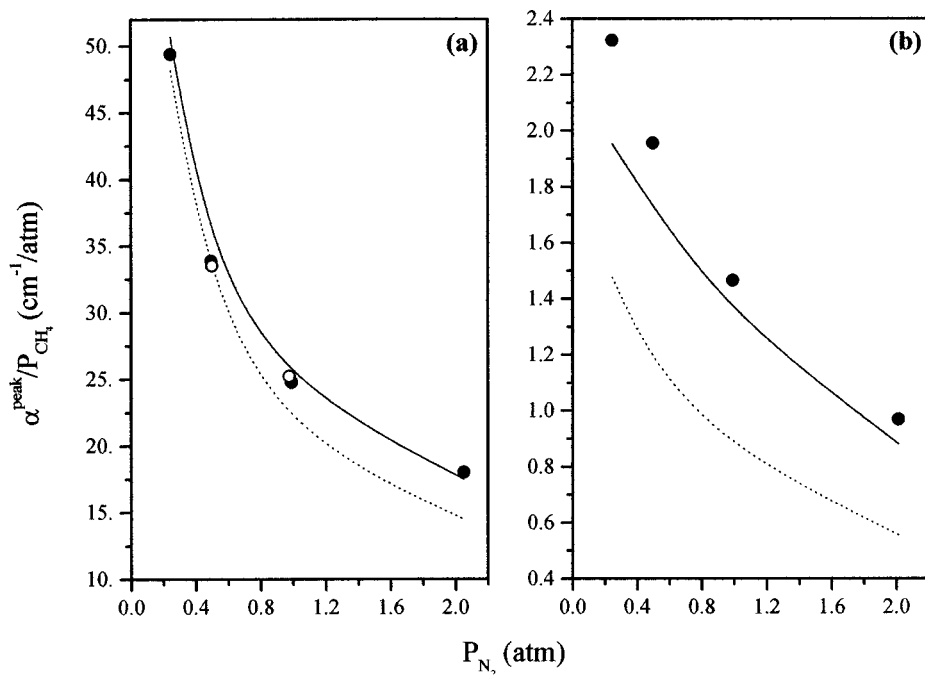FIG. 13. Same as Fig. 10, but for the manifolds; (a) $R(11)$ at 0.973 atm; (b) $R(12)$ at 1.98 atm.

FIG. 14. Effect of pressure on peak absorption in the $R(8)$ (a) and $R(16)$ (b) manifolds. $\bigcirc$ and $\bullet$ are values measured by groups G2 and G3, respectively. — and --- have been calculated with and without the inclusion of line mixing.

stant $A(R,R), A(R,P), \ldots$ parameters. Indeed, previous results for CO_2 (Ref. 13) indicate that interbranch (resp. intrabranch) mixing strongly decrease (resp. increase) with increasing J. Use of a constant intrabranch parameter $A(R,R)$ determined from absorption for $J=8$ should thus lead to underestimation of line-mixing effects for high rotational quantum number manifolds, as observed here. The last reason is the lack of precision of some of the line-broadening coefficients used. Indeed, there is strong evidence that the parameters available,[39] which are estimated values,[41] are too large hence explaining that the widths of high J manifolds are overestimated. Note that other problems remain that have been pointed out; for instance, some line-coupling elements

within the $R(11)$ and $R(12)$ manifolds are clearly overestimated. Finally, it is worth recalling that the present paper confirms that atmospheric spectra are affected by line mixing. This should be accounted for while retrieving methane mixing ratios and computing cooling rates.

Future studies should be based on improved parameters of isolated lines among which half-widths should receive particular attention since they have crucial influence on analysis of line-mixing effects. The effects of temperature should then be studied together with the influence of the collision partner [e.g., He which may have a particular behavior (Refs. 13, 47, 48). These references show that collisions with He lead to effects on CO_2 and N_2O spectra that
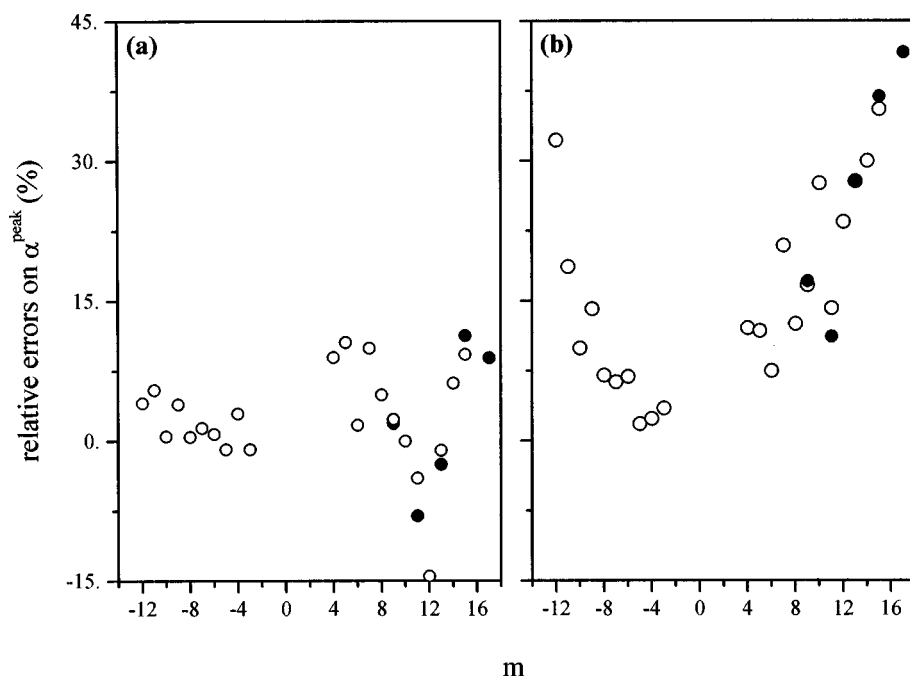

FIG. 15. Relative errors on the computed peak absorption of the ν_3 band features for a pressure of about 1 atm. Values in the R and P manifolds are plotted vs rotational quantum number m. $\bigcirc$ and $\bullet$ are values deduced from measurements by groups G2 and G3, respectively. (a) Results obtained with our model. (b) Results obtained neglecting line mixing.
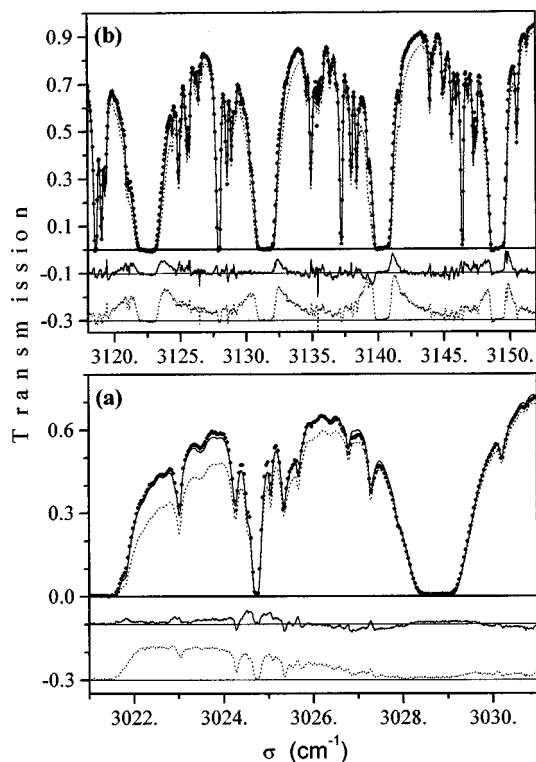
FIG. 16. Transmission in the ν_3 band for the conditions $P_{CH_4} = 8.2 \times 10^{-3}$ atm, $P_{N_2} = 0.985$ atm, and $L = 20.1$ m. ● are measured values; — and --- have been calculated with and without the inclusion of line mixing, respectively. Shifted obs−calc deviations are displayed in the lower part of the plots. (a) High frequency near wing of the Q branch. (b) Region of the $R(10)$−$R(13)$ manifolds.

are different from those induced by collisions with Ar, O_2, and N_2 (the effects of line mixing are significantly more important leading to more narrow profiles), and H_2 which is of interest for application to Jupiter]. Finally, investigations should be made in bands other than ν_3 (e.g., the ν_2, ν_4 dyad for atmospheric emission, and the $2\nu_3$ region which contributes to the absorption of solar radiation). Finally comparison

of the relaxation operators and calculated spectra obtained with the present model and the empirical approach of Ref. 11 might bring useful information on collisional processes. These issues will be considered in forthcoming papers.

ACKNOWLEDGMENTS

APPENDIX A: CH_4−N_2 AND CH_4−Ar COLLISIONS

The model presented in this work starts from semiclassical calculations of collisional state-to-state relaxation rates for the methane−argon system, these data being used for a study of CH_4−N_2 mixtures. Since magnitude scaling factors A have been used [Eq. (6)], our approach assumes that collisional transfers induced by collisions with N_2 and Ar verify

$$K_{j \leftarrow i}^{N_2} = a \times K_{j \leftarrow i}^{Ar} \quad \text{and}$$

$$\text{Re}\{\langle\langle k' | \mathbf{W}^{N_2} | k \rangle\rangle\} = a \times \text{Re}\{\langle\langle k' | \mathbf{W}^{Ar} | k \rangle\rangle\}, \quad (A1)$$

where a is a constant, independent on the quantum states i and j and on the lines k and k'. The lack of detailed data for CH_4−N_2 collisions forbids direct study of the quality of this approximation. Nevertheless, the line broadening parameters γ_k and first order line mixing coefficients Y_k of Ref. 9 enable a first check of Eq. (A1). Indeed, Fig. 17 shows that the ratio of values for Ar and N_2 is practically independent on the considered line. This is an indication that, at least on a global point of view, Eq. (A1) is reasonable since the parameters in Fig. 17 are related with the relaxation operator matrix elements by Eq. (2) and[8,9]

$$Y_k = 2 \times \sum_{k' \neq k} \frac{d_{k'}}{d_k} \times \frac{\text{Re}\{\langle\langle k' | \mathbf{W} | k \rangle\rangle\}}{\sigma_k - \sigma_{k'}}. \quad (A2)$$
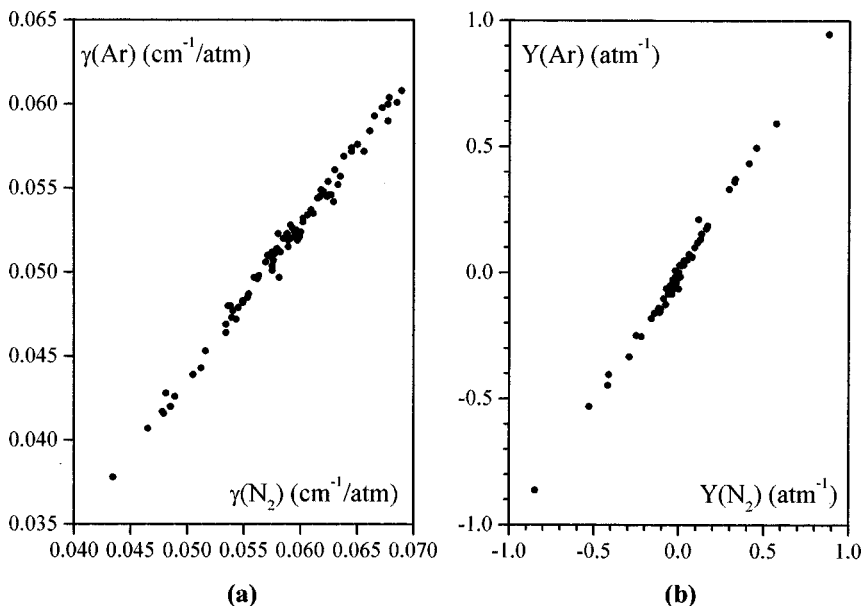

FIG. 17. Comparison between values of collision parameters for CH_4−Ar and CH_4−N_2 collisions. ● are values measured for R and P lines ($J \leq 10$) in the ν_3 band at room temperature (Ref. 9). (a) Line-broadening coefficients γ_k; (b) First order line-mixing coefficients Y_k.

TABLE II. Selection rules of the line-coupling relaxation matrix elements.

$k \backslash k'$	$F_2 \leftarrow F_1$	$F_1 \leftarrow F_2$	$A_2 \leftarrow A_1$	$A_1 \leftarrow A_2$	$E \leftarrow E$
$F_2 \leftarrow F_1$	N	Y	N	N	N
$F_1 \leftarrow F_2$	Y	N	N	N	N
$A_2 \leftarrow A_1$	N	N	N	Y	N
$A_1 \leftarrow A_2$	N	N	Y	N	N
$E \leftarrow E$	N	N	N	N	Y

APPENDIX B: PROPENSITY RULES

Selection rules for rotational energy transfer by collision in spherical-top molecules have been discussed in a number of papers (see Refs. 12, 44, 45, 49, and those therein). Nevertheless, these studies mostly deal with $\Delta J \neq 0$ and little is known on propensity rules for the quasiresonant $\Delta J = 0$ transfers that are involved by line mixing within P and R manifolds.

In Ref. 10, a first collisional selection rule was introduced, which assumes that line mixing between transitions involving states of different (A, E, F) nuclear spin symmetries are negligible. Latter on, Benner *et al.*[11] determined some relaxation matrix elements from fits of laboratory spectra; they empirically found that better agreement between observed and recomputed spectra was obtained when $(A \text{ or } F)_1 \leftarrow (A \text{ or } F)_1$ and $(A \text{ or } F)_2 \leftarrow (A \text{ or } F)_2$ line-coupling (for $\Delta J = 0$) terms were set to zero. The final set of selection rules is then summarized in Table II. We checked if in our model, the same rules hold. That related with the nuclear spin is of course verified since the potential used in the semi classical calculations contains no term permitting transfer between A, E, and F states. In order to check that $1 \leftarrow 1$ and $2 \leftarrow 2$ changes are small, we have considered transfers between levels of a given J value (which compose the R and P manifold). For these states, we have computed the sums

$$ S(J, X, Y) = \sum_{i \in X} \sum_{j \neq i \in Y} \rho_i \times K_{j \leftarrow i} \bigg/ \sum_{i \in X} \rho_i $$
$$ \text{for } X, Y = F_1, F_2 \text{ or } A_1, A_2. \quad \text{(B1)} $$

The numerical values show that the $S(J, X, X)$ parameters are very small (about 2%) when compared with the $S(J, X, Y \neq X)$ thus confirming the conclusion, made in Ref. 11, that $1 \leftarrow 1$ and $2 \leftarrow 2$ transfers within a given J can be neglected. This results from the fact that $1 \leftrightarrow 2$ changes are induced by a third order term of the potential whereas the $1 \leftarrow 1$ and $2 \leftarrow 2$ transitions result from higher rank terms.

Analysis of the results in Figs. 10 and 11 has shown that some F_1 and F_2 lines are largely coupled whereas some others are not. This demonstrates the high selectivity of collisional processes and makes statistically based fitting laws[50] inappropriate for the modeling of line mixing in methane spectra. The widely used exponential gap law, for instance, is given by

$$ K_{j \leftarrow i} = a \times \exp(-b |\Delta E_{j \leftarrow i}|). \quad \text{(B2)} $$

Although parameters a and b depending on the nuclear spin of the i and j levels are used,[34,51] Eq. (B2) will fail in mod-

eling line mixing. Indeed, within a given manifold, $\Delta E_{j \leftarrow i}$ is practically zero; all collisional transfers between F_1 and F_2 lines are then identical (i.e., $K_{j \leftarrow i} = a_{F2,F1}$) in contradiction with the results in Fig. 11(a). The failure of fitting laws was already noted in Refs. 34, 44, 45 but is also confirmed by some results that we have obtained prior to the development of the model presented here. At that time, we used Eq. (B2) and determined the a and b constants from fits of high pressure spectra. Satisfactory results were obtained above 25 atm but the model totally failed in predicting the shape of manifolds at low pressures.

[1] C. Camy-Peyret, J. M. Flaud, A. Perrin, C. P. Rinsland, A. Goldman, and F. J. Murcray, J. Atmos. Chem. **16**, 31 (1993).
[2] M. C. Abrams, G. L. Manney, M. R. Gunson, M. M. Abbas, A. Y. Chang, A. Goldman, F. W. Irion, H. A. Michelsen, M. J. Newchurch, C. P. Rinsland, R. J. Salawitch, G. P. Stiller, and R. Zander, Geophys. Res. Lett. **23**, 2341 (1996).
[3] D. Gautier, B. Bézard, A. Marten, J. P. Baluteau, N. Scott, A. Chedin, V. Kunde, and R. Hanel, Astrophys. J. **257**, 901 (1982).
[4] T. Gabard, J. Quant. Spectrosc. Radiat. Transf. **59**, 287 (1998).
[5] G. Millot, B. Lavorel, and J. I. Steinfeld, J. Chem. Phys. **95**, 7938 (1991).
[6] A. S. Pine, J. Chem. Phys. **97**, 773 (1992).
[7] D. C. Benner, C. P. Rinsland, V. M. Devi, M. A. H. Smith, and D. Atkins, J. Quant. Spectrosc. Radiat. Transf. **53**, 705 (1995).
[8] P. W. Rosenkranz, IEEE Trans. Antennas Propag. **AP-23**, 498 (1975).
[9] A. S. Pine, J. Quant. Spectrosc. Radiat. Transf. **57**, 157 (1997).
[10] A. S. Pine, J. Quant. Spectrosc. Radiat. Transf. **57**, 145 (1997).
[11] V. M. Devi, D. C. Benner, M. A. H. Smith, C. P. Rinsland, G. Guelachvili, and L. R. Brown, *53rd International Symposium on Molecular Spectroscopy*, paper WF10-WF12, Columbus, Ohio, 1998 (unpublished).
[12] T. Gabard and J.-P. Champion, J. Quant. Spectrosc. Radiat. Transf. **52**, 303 (1994).
[13] R. Rodrigues, B. Khalil, R. Le Doucen, L. Bonamy, and J. M. Hartmann, J. Chem. Phys. **107**, 4118 (1997).
[14] A. Valentin, Spectrochim. Acta A **51**, 1127 (1995).
[15] J. L. Domenech, Ph.D. thesis, Madrid, 1990.
[16] J. Santos, P. Cancio, J. L. Doménech, J. Rodriguez, and D. Bermejo, Laser Chem. **12**, 53 (1992).
[17] P. Cancio and D. Bermejo, J. Opt. Soc. Am. B **14**, 1305 (1997).
[18] A. Ben-Reuven, Phys. Rev. **145**, 7 (1966).
[19] E. W. Smith, J. Chem. Phys. **74**, 6658 (1981).
[20] F. Rachet, M. Margottin-Maclou, A. Henry, and A. Valentin, J. Mol. Spectrosc. **175**, 315 (1996).
[21] L. L. Strow, D. C. Tobin, and S. E. Hannon, J. Quant. Spectrosc. Radiat. Transf. **52**, 281 (1994).
[22] R. Rodrigues, P. De Natale, G. Dilonardo, and J. M. Hartmann, J. Mol. Spectrosc. **175**, 435 (1995).
[23] Q. Ma, R. H. Tipping, G. Birnbaum, and C. Boulet, J. Quant. Spectrosc. Radiat. Transf. **59**, 259 (1998).
[24] T. Gabard, Ph.D. thesis, Université de Bourgogne, Dijon, France, 1996.
[25] T. Gabard, J. Quant. Spectrosc. Radiat. Transf. **57**, 177 (1997).
[26] D. V. Kalinin, D. K. Bronnikov, Yu. G. Selivanov, T. Gabard, J.-P. Champion, and J.-C. Hilico, J. Quant. Spectrosc. Radiat. Transfer (in press).
[27] T. G. Heil and D. Secrest, J. Chem. Phys. **69**, 219 (1978).
[28] U. Buck, J. Schleusener, D. J. Mailk, and D. Secrest, J. Chem. Phys. **74**, 1707 (1981).
[29] L. N. Smith and D. Secrest, J. Chem. Phys. **74**, 3882 (1981).
[30] G. Jolicard and M.-Y. Perrin, Chem. Phys. **81**, 135 (1983).
[31] M.-Y. Perrin and G. Jolicard, Chem. Phys. **91**, 341 (1984).
[32] M. M. Szczesniak, G. Chajasinski, and S. M. Cybulski, J. Chem. Phys. **96**, 463 (1992).
[33] D. J. Nesbitt, J. W. Nibler, A. Schiffman, W. B. Chapman, and J. M. Hutson, J. Chem. Phys. **98**, 9513 (1993).
[34] W. B. Chapman, A. Schiffman, J. M. Hutson, and D. J. Nesbitt, J. Chem. Phys. **105**, 3497 (1996).
[35] T. G. A. Heijmen, T. Korona, R. Moszynski, P. E. S. Worner, and A. Van Der Avoird, J. Chem. Phys. **107**, 902 (1997).
[36] U. Buck, K. H. Khol, A. Kohlhase, M. Faubel, and V. Staemmler, Mol. Phys. **55**, 1255 (1985).

[37] T. Phillips and D. Secrest, J. Chem. Phys. **91**, 2840 (1989).

[38] C. Boursier, F. Menard-Bourcin, and C. Boulet, J. Chem. Phys. **101**, 9589 (1994).

[39] L. S. Rothman, ASA meeting, Reims, France, 4–6 September, 1996.

[40] D. C. Benner, V. Malathy Devi, M. A. H. Smith, and C. P. Rinsland, J. Quant. Spectrosc. Radiat. Transf. **50**, 65 (1993).

[41] L. R. Brown, J. S. Margolis, J. P. Champion, J. C. Hilico, J. M. Jouvard, M. Loete, C. Chackerian, Jr., G. Tarrago, and D. C. Benner, J. Quant. Spectrosc. Radiat. Transf. **48**, 617 (1992).

[42] M. V. Tonkov, J. Boissoles, R. Le Doucen, B. Khalil, and F. Thibault, J. Quant. Spectrosc. Radiat. Transf. **55**, 321 (1996).

[43] J.-M. Hartmann, J.-P. Bouanich, K. W. Jucks, Gh. Blanquet, J. Walrand, D. Bermejo, and J.-L. Domenech, J. Chem. Phys. **110**, 1959 (1999).

[44] B. Foy, J. Hetzler, G. Millot, and J. I. Steinfeld, J. Chem. Phys. **88**, 6838 (1988).

[45] J. J. Klaassen, S. L. Coy, J. I. Steinfeld, and Bernd Abel, J. Chem. Phys. **101**, 10533 (1994).

[46] R. Rodrigues, K. W. Jucks, N. Lacome, Gh. Blanquet, J. Walrand, W. A. Traub, B. Khalil, R. Le Doucen, A. Valentin, C. Camy-Peyret, L. Bonamy, and J. M. Hartmann, J. Quant. Spectrosc. Radiat. Transfer **61**, 153 (1999).

[47] R. Rodrigues, C. Boulet, L. Bonamy, and J. M. Hartmann, J. Chem. Phys. **109**, 3037 (1998).

[48] J. P. Bouanich, J. M. Hartmann, G. Blanquet, J. Walrand, D. Bermejo, and J. L. Domenech, J. Chem. Phys. **109**, 6684 (1998).

[49] R. Parson, J. Chem. Phys. **93**, 8731 (1990); **95**, 5492 (1991).

[50] T. A. Brunner and D. Pritchard, in *Dynamics of the Excited State*, edited by K. P. Lawley (Wiley, New York, 1982), pp. 589–641.

[51] J. R. Hetzler and J. I. Steinfeld, J. Chem. Phys. **92**, 7135 (1990).